Russian Journal of Earth Sciences

Comparative Analysis of the Unmanned Aerial Vehicles and Terrestrial Laser Scanning Application for Coastal Zone Monitoring

Aleksandr Danchenkov*[,1,2] and Nikolay Belov[2]

[1]Shirshov Institute of Oceanology, Russian Academy of Sciences, Moscow, Russia
[2]Immanuel Kant Baltic Federal University, Kaliningrad, Russia
***Correspondence to:** Aleksandr Danchenkov, aldanchenkov@mail.ru

Abstract: The shallow sandy shores of the tideless sea are regularly affected by storm activity. Foredune ridge is a natural and anthropogenic object, a natural protective barrier that protects ecosystems and populated areas from the effects of dangerous hydrometeorological phenomena such as storm surges and wind-sand flux. In the course of impact of dangerous hydrometeorological phenomena, the foredune ridge integrity is disturbed, the composing material is washed away thus forming breakthroughs. Monitoring of the foredune state is an important stage in maintaining its condition and also provides an empirical basis for predicting the impact of hazardous events. The use of ground-based laser scanning technology as well as digital photogrammetry for the study of sensitive coastal zones is justified for these purposes. In this article, we compare the results of calculating the dynamics of the beach sand material and advance them according to the results of ground-based laser scanning and digital photogrammetry. Comparability is provided by high-density clouds of ground-scan points and digital photogrammetry in a single coordinate reference. Two sections of the sensitive coastal zone of the Curonian Spit (Russian sector of the South-Eastern Baltic) have been explored in advance. A comparison of the applicability of means for obtaining digital elevation models to evaluate the dynamics of sand material has been made. In comparison with TLS, the use of UAV with the SfM algorithm is limited to post-storm surveys, since the final accuracy does not provide for reliable lithodynamic studies due to the small scale of processes comparable to measurement errors.

Keywords: coast, monitoring, UAV, TLS, DGPS, photogrammetry, DEM/DTM

Citation: Danchenkov, A., Belov N. (2023), Comparative Analysis of the Unmanned Aerial Vehicles and Terrestrial Laser Scanning Application for Coastal Zone Monitoring, *Russ. J. Earth. Sci.*, 23, ES4008, https://doi.org/10.2205/2023es000854

Research Article

Received: 17 October 2022
Accepted: 26 May 2023
Published: 25 November 2023

1. Introduction

1.1. Monitoring of Changes in the Coastal Zone

The use of airborne LIDAR to obtain digital terrain models in the coastal zone has been predominant in various studies [*Gonçalves and Henriques*, 2015; *Haala et al.*, 2013]. A relatively small post-processing of results has made this technology widely applicable to assess the volume of changes and morphodynamics of the coastal zone, in particular beaches and coastal dunes [*Dudzińska-Nowak and Wężyk*, 2014; *Kempeneers et al.*, 2009; *Mitasova et al.*, 2005, 2009; *Pe'eri and Long*, 2011; *Sallenger Jr. et al.*, 2003; *White and Wang*, 2003; *Xhardé et al.*, 2011]

The development of digital photography has resulted in the use of digital photogrammetry for onshore research. The use of high-precision referencing using DGPS, as well as technologies for converting stereopairs of photographs into 3D point clouds allows creating sufficiently accurate digital terrain models, which was previously possible only with the use of airborne LIDAR [*Gonçalves and Henriques*, 2015; *Haala*, 2009].

The technology of ground-based laser scanning (ground LIDAR system) for the purposes of monitoring the coastal zone allows for obtaining high-precision clouds of survey points and using 3D modeling, especially for sections of the coast with complex morphology. This technology is widely used in studies of various natural objects (vegetation cover [*Bienert et al.*, 2006], water objects [*Brasington et al.*, 2012; *Hodge et al.*, 2009], research and monitoring of landslide processes [*Abellán et al.*, 2011; *Abellán et al.*, 2006; *Rowlands et al.*, 2003; *Travelletti et al.*, 2008], coastal zones [*Collins and Sitar*, 2005; *Poulton et al.*, 2006; *Sergeev et al.*, 2016], coastal dunes and beaches [*Danchenkov*, 2016; *Danchenkov et al.*, 2019; *Danchenkov and Belov*, 2019; *Fabbri et al.*, 2017; *Lee et al.*, 2011, 2016].

The most dangerous hydrometeorological phenomena on the southeastern coasts of the Baltic Sea are frequently associated with strong and stormy winds [*Danchenkov et al.*, 2023]. Currently, there is a change in various climatic characteristics: an increase in the number of storm days and the speed of storm winds [*Stont*, 2014; *Stont et al.*, 2020]. The most common effects of annual seasonal storms are wave erosion of the windward slopes of the dune rampart and primary leaning aeolian forms, with subsequent activation of gravitational processes and sand redeposition [*Bobykina and Stont*, 2014, 2015; *Danchenkov et al.*, 2019]. Intensive deflation in the blowouts and transit of sand from the beach to the closest forests is also frequent aftermath. Storms of higher intensity (recurrence once in 25–50 years) may cause much more dramatic changes, up to breakthroughs of the foredune ridge and flooding of the inland territory [*Bobykina and Stont*, 2015; *Boldyrev et al.*, 2008; *Danchenkov et al.*, 2023; *Kirlis*, 1971].

The largest coastal accumulative form on the southeast coast of the Baltic Sea is the Curonian Spit. The spit is stretched in the northeastern direction, ending at a narrow (400–650 m) strait opposite the city of Klaipeda. The Curonian Spit is 98 km long, 49 of which are located on the territory of the Kaliningrad region, and 47 km are within the borders of the national park. The width of the Curonian Spit varies from 3800 m near the village of Nida to 410 m by the 12th km. The spit is shaped as a shallow arc on the plan.

To monitor the impact of dangerous hydrometeorological phenomena on the stability of foredune ridges and beaches on the coast of accumulative spits of the Russian sector of the Southeastern Baltic, digital terrain models can be created using photogrammetric technologies, which, however, requires a preliminary comparison of their quality with other means of obtaining planned and high-altitude data. From 2014 to 2018, regular measurements using ground-based laser scanning (TLS) with a resolution of 3.5×3.5 cm have been performed at the 14th kilometers (Test site A) and 42nd kilometers of the spit (Test site B) (more than 70 measurements) on two model sections of the Curonian Spit (Kaliningrad Oblast). Orthophotography was also carried out in these sections using an unmanned aerial vehicle DJI Phantom 4, with an FC330 camera. The use of unmanned aerial vehicles (UAVs) was determined by the goal of the potential increase in the foredune state monitoring sites, as well as the production of more mobile and urgent measurements, primarily post-storm measurements, with a reduction in their cost. In this study, the main goal was to compare the accuracy of the data obtained with the use of UAV with the data obtained as a result of TLS. UAVs have already proven themselves for small areas mapping, including coastal zone [*Chang et al.*, 2021; *Eisenbeiss*, 2011; *Gonçalves and Henriques*, 2015; *Jeyaraj et al.*, 2022; *Remondino et al.*, 2011; *Turner et al.*, 2016; *Zanutta et al.*, 2020].

1.2. A Brief Review of UAV Technology Application in Scientific and Practical Activities

For a long time, UAVs application has been associated with the military industry [*Gonçalves and Henriques*, 2015]. The intensive development of technology, however, has led to the emergence of companies that produce a wide range of devices for civilian use in various fields of activity. Their cost and technical characteristics, in particular weight, camera equipment, operating time, as well as a high degree of the operation process automation, provided a wide potential for use in a number of areas, such as geological mapping [*Johnson et al.*, 2014], archaeological studies [*Rinaudo et al.*, 2012] and forestry

[*Puliti et al.*, 2015] A summary of information on the use of UAVs for photogrammetry and remote sensing has already been provided in several studies [*Colomina and Molina*, 2014; *Nex and Remondino*, 2013]. The use of UAVs with the view to study the coastal zone is described in only a few studies in the form of an accuracy estimate of such GCP (Ground control point) studies obtained using DGPS/RTK [*Delacourt et al.*, 2009; *Gonçalves and Henriques*, 2015; *Turner et al.*, 2016].

1.3. A Brief Overview of Comparisons of Processing Results of Aerial Photographs Using the Structure-From-Motion (SfM) Method and TLS Results

The development of digital image processing technologies using Structure-from-Motion (SfM) computer vision algorithms, coupled with the availability of UAVs equipped with consumer-grade digital cameras, resulted in the widespread use of these technologies for the remote observations of the environment and its monitoring [*Clapuyt et al.*, 2016; *Neitzel and Klonowski*, 2011]. The SfM technology makes it possible to reconstruct the topographic surface of the survey area based on many digital images, including those obtained with UAVs equipped with a consumer-grade camera. The SfM algorithm is aimed at reconstructing the structure of the 3D scene, based on the correspondences of the intersecting digital images *Clapuyt et al.* [2016], *Snavely et al.* [2007]. The reconstruction result is a point cloud, in an arbitrary coordinate system (or UAV internal GPS system). Exact coordinate fixing is carried out through ground control points (GCP), which were obtained using DGPS/RTK [*Clapuyt et al.*, 2016]. A comparison of the accuracy of the work was previously carried out in several studies. In this study [*Westoby et al.*, 2012], the TLS survey of the coastal ledge and SfM results were compared. The result of the comparison showed an absolute accuracy of 0.5 m. It is also demonstrated by the example of the coastal ledge, by *James et al.* [2012] that RMSE between the TLS and SfM results was 0.07 m. The comparison of UAV and NLS results was already provided by the example of the river valley [*Cook*, 2017].

2. Materials and Methods

2.1. Test Sites

Two test sites ("A" and "B") are located on the territory of the Curonian Spit, the Kaliningrad region, at the 14th ("A") and 42nd ("B") kilometers of its extent were selected for this study (Figure 1). Both sites are fragments of the sea coast of a large spit, separating the Baltic Sea water area from the shallow fresh lagoon (Curonian Lagoon).

The variability of the foredune of the Curonian Spit is of pulsating character [*Badyukova et al.*, 2017]. Open areas are most likely to undergo eolian processing; the sections are covered with vegetation – to a lesser extent. The test site "A" consists of two main morphological elements – a shallow sea beach and a developed coastal foredune, the sea slope of which was eroded during the autumn-winter storms of 2014–2015, the site is lithodynamically active, mainly in terms of erosion and deflation. The test site "B" is composed of three main morphological forms – a flat sea beach, an embryonic dune and a foredune densely covered with vegetation. The "B" site has an active embryo dune that periodically erodes. [*Morozov and Petrov*, 2010].

The sites have been regularly inspected for several years, mostly using TLS. The data from previous surveys give an idea of the intensity of the occurrence of lithodynamic processes in the sites, which will allow us to assess the applicability of UAVs for monitoring the condition of the shallow sandy beach and the foredune ridge.

2.2. The DJI Phantom 4

DJI Phantom 4 was used for this study which relates to the UAV customer class. DJI Phantom 4 has the following characteristics – quadrocopter (4 propellers); the maximum climb speed is 6 m/s; the maximum flight speed is 20 m/s; built-in sensors – GPS, GLONASS; type of control – radio channel; a range of control – 3500 m (radio channel); weight – 1380 g; Characteristics of FC330 camera are 1/2.3"CMOS camera, the number of

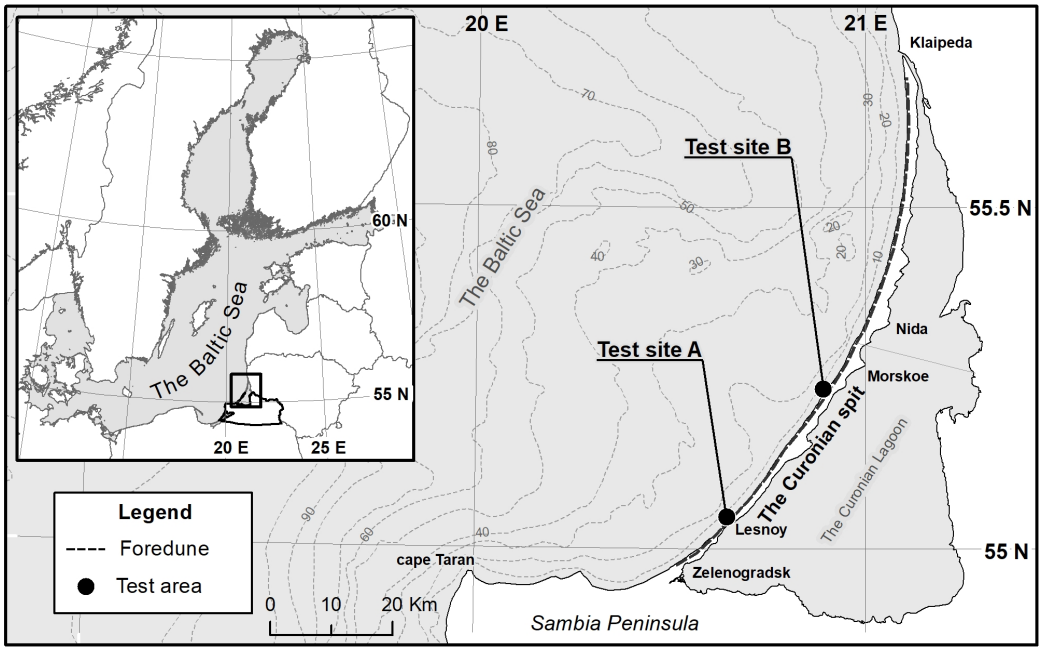

Figure 1. Locations of the two test sites on the Baltic Sea coast (The Curonian spit).

effective pixels: 12 Mpx; lens angle of view – 94° (20 mm (equivalent to 35 mm format), f/2.8, focus on ∞); photography resolution – 4000 × 3000 px.

The quadrocopter is powered by a small Li-ion battery, the operating time of which essentially depends on weather conditions (ambient temperature, wind force) and is maximally 28 minutes long.

The quadrocopter was equipped with FC330 stock camera from the delivery set, with 12 Mpx resolution (4000 × 3000 px), physical size of the sensor is 6.24 mm, and the focal length is 3.61 mm. For a flight altitude of 40 m, GSD is 1.73 cm/px (Pix4D GSD Calculator).

The camera was calibrated according to a pre-prepared target from a distance of 1 m. The peculiarity of cameras with electronic shutters is the need to calibrate each time before departure.

2.3. UAV and GCP Data Acquisition and Processing

Two flight missions were performed for this study, one for each test site. The day of the survey (April 10, 2018) was chosen on the basis of the most favorable meteorological situation – wind speed of 2 m/s, northeast direction. Such meteorological parameters do not cause significant eolian processes of sand material transfer or wave erosion of beaches for the study area, which may introduce errors in the measurement results. On the day of measurements, the range of visibility was 4 km, air temperature 9 °C, and high cloudiness (2–2.5 km) less than 10%, which created favorable conditions for flights and aerial photography. The surveys were carried out in the period of 10 am–1 pm, synchronously with the TLS measurements, to reduce the probability of changes in the volume of sand material in the test sites.

The size of test sites of 170 × 90 m ("A", 14 km) 170 × 80 m ("B", 42 km) provided for shooting within one pilot mission for each of the sites. Ground targets of GCP were placed and fixed before the flight. The pilot mission was carried out using Pix4Dcapture autopilot. 191 aerial photographs were obtained for the test site "A", and 149 aerial photographs for the site "B" from a flight altitude of 40 m, which took 14 and 15 minutes, correspondingly. The photography was done automatically by creating a double grid flight plan in Pix4Dcapture autopilot. The direction of shooting was strictly nadir (90°). Figure 2 shows the overlapping of photos in the test sites, as well as the camera position when taking photographs. Most of the area of the sites is covered with individual photographs more than 9 times, which makes it possible to effectively obtain a point cloud during processing.

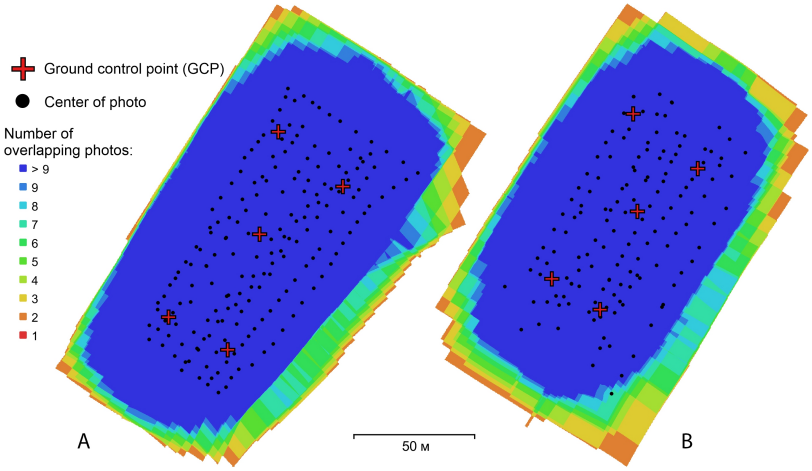

Figure 2. Photo images overlaps and UAV camera locations. A – test site "A", B – test site "B". The legend on the left represents count of photographs overlapping.

A ground control point (GCP) system of five targets was used to coordinate aerial photography – four targets were located at the corners of the site and one in the center. The distance between the nearest targets was 40–70 meters. For small shooting areas, five GCPs are sufficient to orient the images. [*Nocerino et al.*, 2013].

In natural areas, including the test sites, it is rather difficult to distinguish remarkable easily and unambiguously defined points, in order to use them as GCP targets. In view of this, pre-fabricated targets were used for aerial photography. The targets were produced via printing on a dense banner fabric made of reinforced polyvinylchloride of 1×1 meters (Figure 3B). To simplify the determination of the target center in aerial photographs, a red cross, 0.15 m thick, was printed on a white banner fabric with a centered system of circles in the center. There is also a typographic eye watch (eyelet) in the center of the cross, for precise adjustment of a mark with a GNSS antenna. Each target made of banner fabric is numbered with an ordinal number in Myriad font, digit height is 0.2 m (Figure 3B, 3C) for visual interpretation from aerial photographs.

The target coordinates were determined using TOPCON GR-5 satellite geodetic equipment in RTK mode (Figure 3B). The differential correction was obtained from the network of base stations. Coordinate system projected by WGS84 UTM34N. The accuracy of determination of plan coordinates (x, y) was 0.01 m, and 0.015 m for elevation (z).

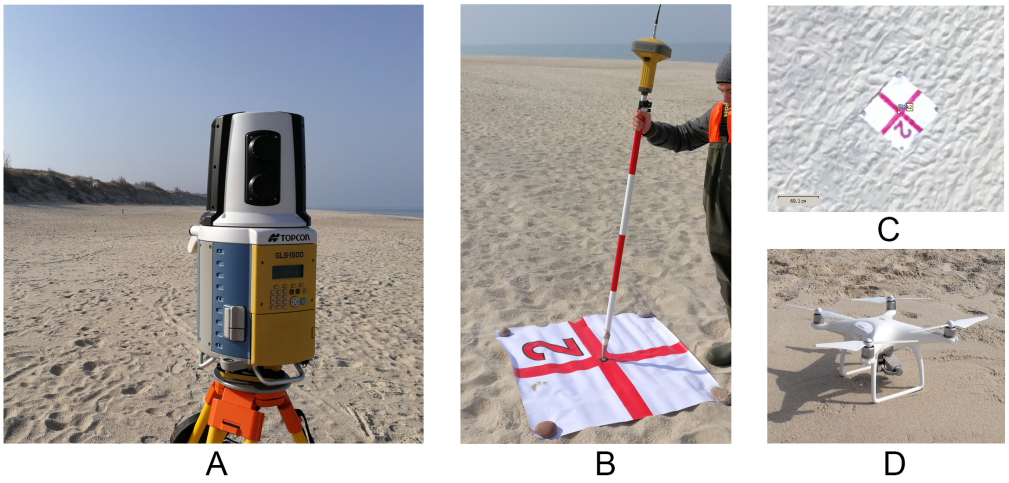

Figure 3. A – TOPCON GLS-1500 during scanning; B – Ground target number 2 and preparation to obtain its coordinates using TOPCON GR-5; C – the same target on aerial photo; D – DJI Phantom 4 before the flight mission.

The data collected during the UAV mission was post-processed using Agisoft PhotoScan software, which enables us to receive various digital products through photogrammetric analysis of digital images. The software applies SfM technology, which is also used in several similar programs [*Furukawa and Ponce*, 2010; *Gonçalves and Henriques*, 2015; *Pierrot Deseilligny and Clery*, 2011]. Agisoft PhotoScan is an automated 3D surface reconstruction tool for digital photography [*Agisoft*, 2018]. This software is based on standard and published algorithms, and the workflow is well documented in *Gonçalves and Henriques* [2015] study.

2.4. Terrestrial Laser Scanning and Data Acquisition

The measurements using ground-based laser scanning (TLS) technology were used for independent estimation of the accuracy of the SfM method for studying the dynamics of shallow sandy sea shores. The data was collected using the topographic laser scanner TOPCON GLS-1500 (Figure 3A). The accuracy of determination of distances and angles is 4 mm for 150 mm of measurements, and the angular accuracy is 6". The scanning system makes it possible to obtain data in the form of XYZ coordinates, the intensity of the laser beam reflection from the surface, as well as RGB dot colors. The scanning system is equipped with a sensor system for self-calibration and elimination of level errors, a collimator, and a rotation system started before each launch which does not require manual calibration [*Topcon*, 2010].

Co-registration of TLS data was performed by the back-sight method using the target (BS) installed on the tripod, as well as the GNSS receiver TOPCON GR-5. The differential correction was obtained from the internal network of base stations. For registration, the scanning system TOPCON GLS-1500 makes polar measurements of target coordinates (BS), from each of the standpoints (OCC1, OCC2). Using the GNSS receiver sequentially installed strictly in the tribrach TOPCON GLS-1500, as well as the target tracker, the coordinates of scanner positions (OCC1, OCC2) were obtained, in fixed mode with a target and altitude accuracy of 0.01 and 0.015 m, respectively. The projected WGS84 UTM34N coordinate system was used, likewise in the case of making measurements in GCP during the UAV DJI Phantom 4 mission.

Fieldwork was carried out on April 10, 2018, on two sections of the Curonian Spit different in morphology. Two scanning stations were performed in both test sites, with a total area of 1.07 ha and 0.99 ha, respectively. The location of stations was chosen based on the minimization of blind zones, to obtain complete coverage of the sites. The shooting resolution was 35×35 mm at 10 m distance from the scanning system.

3. Results

3.1. Image Orientation, Geo-Referencing and Point Cloud Generation

Processing of digital images based on the UAV mission results in both test sites was performed in WGS84 UTM34N system according to the standard working algorithm. The images were oriented automatically. The alignment mode was chosen as "High", with pre-selection by reference from EXIF properties of the photo (via built-in UAV sensors), in conjunction with the general pre-selection. The number of characteristic points per frame was set at 100,000, and the connecting frame of the points is not less than 10,000. The results of photo alignment are shown in Table 1.

Table 1. Alignment results of digital photos

Test site	Number of used aerial photographs	Number of tie points	Number of projections	RMSE (pixels)
"A"	187	110824	1523268	1.000
"B"	143	93800	956633	0.879

As a result of alignment, the number of aerial photographs used has been reduced, since some of them involved the water surface. Constantly changing its position sea disturbance does not provide for high-quality processing of aerial photographs and introduces additional errors in processing. The alignment error was within 1 px, with a slight increase in test site "A", which is supposedly due to low overlapping in the photographs of the corner portions of the studied area.

The camera orientation process also includes self-calibration of the camera. The following parameters are subject to calibration: focal length in pixels (f), coordinates of the main point; i.e. coordinates of the intersection of the optical axis of the objective with the sensor plane (cx, cy); coefficients of affinity and slope ($b1$, $b2$); coefficients of radial distortion ($k1$, $k2$, $k3$, $k4$); coefficients of tangential distortion ($p1$, $p2$, $p3$, $p4$).

Geo-referencing was carried out in manual mode, by the method of direct correspondence of GCP shooting with their position in the photographs. This method is more accurate than referencing a ready-made cloud of points to the coordinate system [*Turner et al.*, 2012]. GCP coordinates obtained with GNSS shots in RTK mode was imported in Agisoft PhotoScan. Each aerial photo (187 for site "A", 143 for site "B") included a visual search and placement of markers on ground targets carried out per the numbering. After completion of the matching procedure, the camera position was optimized. The accuracy of the final referencing is presented in Table 2.

Table 2. Images geo-referencing errors at both test sites (in centimeters)

GCP	East error	North error	H error	Total	Placement error (in px)
Test site "A"					
k1	1.646	−0.287	0.284	1.694	0.494
k2	−1.832	0.776	0.412	2.032	0.513
k4	1.879	−0.661	0.057	1.993	0.420
k3	−0.621	0.017	−0.520	0.810	0.499
k5	−1.725	−0.055	−0.387	1.769	0.575
Total	1.610	0.474	0.367	1.718	0.505
Test site "B"					
k1	5.187	−5.464	−0.345	7.541	0.370
k2	6.158	−1.239	1.130	6.382	0.590
k3	−6.560	−0.956	0.696	6.666	0.378
k4	−3.261	2.584	−1.116	4.307	0.629
k5	−2.122	4.858	−0.457	5.321	0.447
Total	4.960	3.538	0.817	6.147	0.502

The total number of targets presented for geo-referencing in test site "A" (187 photographs) was 185 units; 150 units for 143 photos of site "B". The overall accuracy of geo-referencing for site "A" exceeds the accuracy of the test site "B" by a factor of three (mainly due to the plan coordinates), which may be related to RTK differential correction errors, due to the difference in distance from the base station (25 versus 55 km). The marker positioning error is less than one pixel, which may indicate the accuracy and precision in setting correspondences on shots during referencing.

After referencing and optimizing the camera position, point clouds were generated to be subsequently transferred to ESRI ArcGIS 10.0 in XYZ ASCII format to be compared with TLS results. We used the average reconstruction density strategy together with the aggressive filtering method with subsequent manual cleaning. The density of point clouds after the cleaning was 11–35 points/m^2, and their total number was practically the same (263,966 and 249,013 points).

3.2. Terrestrial Laser Scanning and Point Cloud Processing

Processing of TLS field data, registration and coordinate referencing were carried out using Topcon ScanMaster version 2.7. The scans were registered using the coordinates of control points – scanner standing points (OCC1, OCC2), as well as the target (BS) obtained through GNSS measurements. Referencing errors are shown in Table 3.

Table 3. Images geo-referencing errors at both test sites (in centimeters)

Reference point	East error	North error	H error
Test site "A"			
OCC1	0.015	0.020	0.012
OCC2	0.022	0.017	0.021
BS	0.032	0.024	0.018
Test site "B"			
OCC1	0.092	0.057	0.030
OCC2	0.076	0.062	0.027
BS	0.071	0.031	0.021

The accuracy of the coordinate referencing is within one centimeter, which makes it possible to obtain accurate data for the relief surface reconstruction. There is a slight decrease in accuracy at site "B", likewise in the processing of UAV results. The noise was cleared in manual mode, without cleaning the vegetation. Single irregular point clouds were obtained for each area and exported to ASCII XYZ. The number of points was 584,956 points for "A" and 601,238 points for "B".

3.3. Digital Elevation Models (DEM) Generation

The irregularity of the point cloud does not allow us to directly calculate high-altitude errors, which was the reason for regularization (GRID reconstruction). To compare the results of SfM processing with TLS data, digital elevation models by point clouds were made using ArcGIS 10.0 with the Natural Neighbor tool, which implements linear interpolation of point data [*Sibson*, 1981]. The GRID cell size was chosen as 0.2 m according to *Hengl* [2006] approach. The resulting digital elevation models are shown in Figure 6 for comparison.

Fragments were cut off out of the resulting interpolated digital elevation models, where there are stair approaches equipped by the national park to cross the foredune, with the view to exclude these areas from comparison.

4. Discussion and Conclusion

The study of a sandy coastline involved a comparison of TLS and SfM results using the construction of a DEM of difference (DOD). This approach was necessary due to the relatively flat nature of the shoreline, which lacks significant local elevation differences typically found in rocky areas or gorges. The DOD method has been utilized in several studies [*James et al.*, 2012; *Milan et al.*, 2007, 2011]. The DOD was created by subtracting a raster DEM based on SfM from a TLS-constructed DEM. A comparison was made between the elevation values for 166,563 cells at site "A" and 195,538 cells at site "B". Figure 5 depicts the DOD schemes. Three main error estimation areas were identified for separate analysis, the beach, foredune, and vegetation, with error frequency histograms plotted (Figure 6).

The most notable differences in altitude between TLS and SfM, which were observed in the extremes of both test sites, were related to areas covered by vegetation, as previously noted by *Westoby et al.* [2012]. Additionally, for the test site "A", these discrepancies were characterized by a low error repeatability of greater than 0.075 m (26%) for vegetation between 0.3–0.6 m high (comprising shrubs and tall grasses that were not vegetating at the

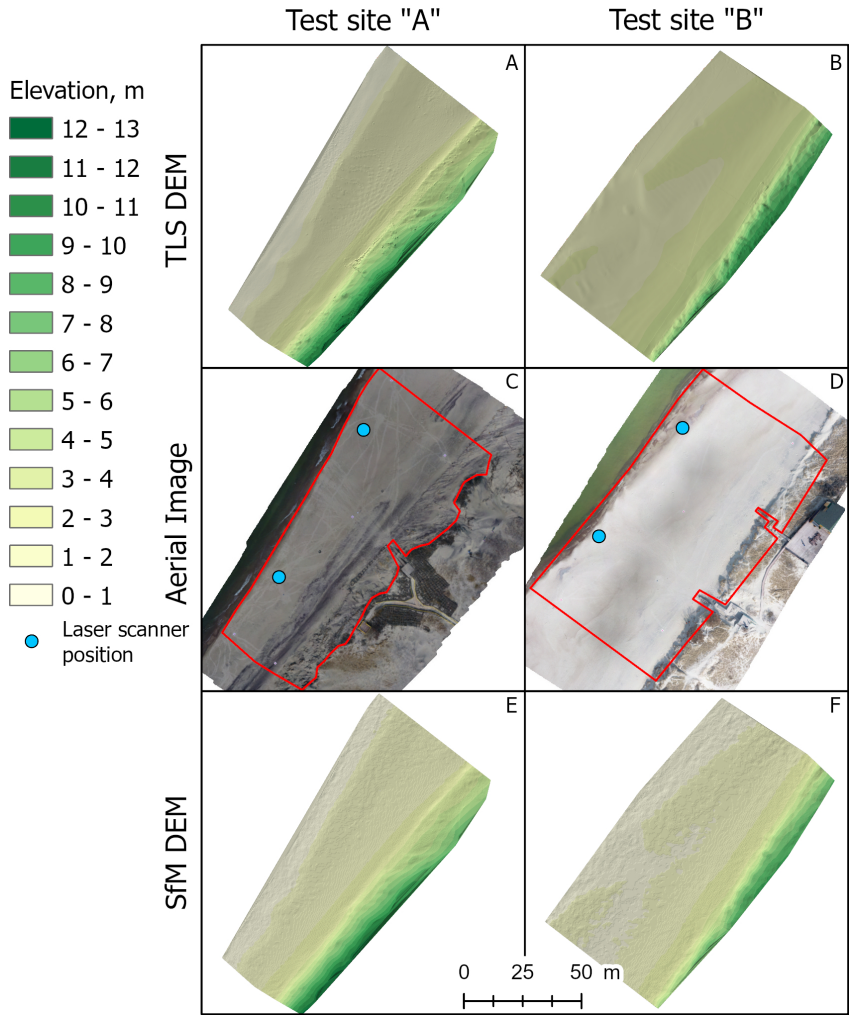

Figure 4. Final interpolated DEMs of test sites; A – site "A" by TLS, B – site "A" by SfM, C – site "B" by TLS, D – site "B" by SfM.

time of measurement). However, for the test site "B", where grass vegetation was growing on the foredune slopes at heights of 0.2–0.4 m high, the error rate of more than 0.075 m exceeded 80%. These differences can be attributed to the limited applicability of both methods for capturing vegetation-covered areas, as noted by *Lane et al.* [2000] for digital photogrammetry and by *Coveney and Fotheringham* [2011] for TLS.

Although the SfM method was found to be applicable for accurately capturing point clouds for river shoals when refraction correction was applied, as described by *Westaway et al.* [2000], it did not demonstrate correct operation (i.e., no correction was performed) in the pre-cut zone of the sea during this experiment. Therefore, all the calculated SfM points below sea level were removed from the point cloud for comparison purposes. However, the presence of water led to significant uncertainties (0.15 to 0.25 m) in the swash zone, as evident in Figure 5A.

The RMSE for the test sites were 0.058 m and 0.097 m, respectively, while the average elevation error was 0.002 m and −0.005 m. The overall errors were consistent with previous studies that compared UAV and TLS, as reported by *Westoby et al.* [2012], [*James and Robson*, 2012], and *Obanawa et al.* [2014], and summarized by *Clapuyt et al.* [2016]. Table 4 provides the complete statistics of elevation errors by zones.

The statistical errors in height measurements presented in Table 4 for different zones correlate with errors in previous studies, even those that used GNSS for comparison [*Gonçalves and Henriques*, 2015; *Turner et al.*, 2012]. There were many points with low

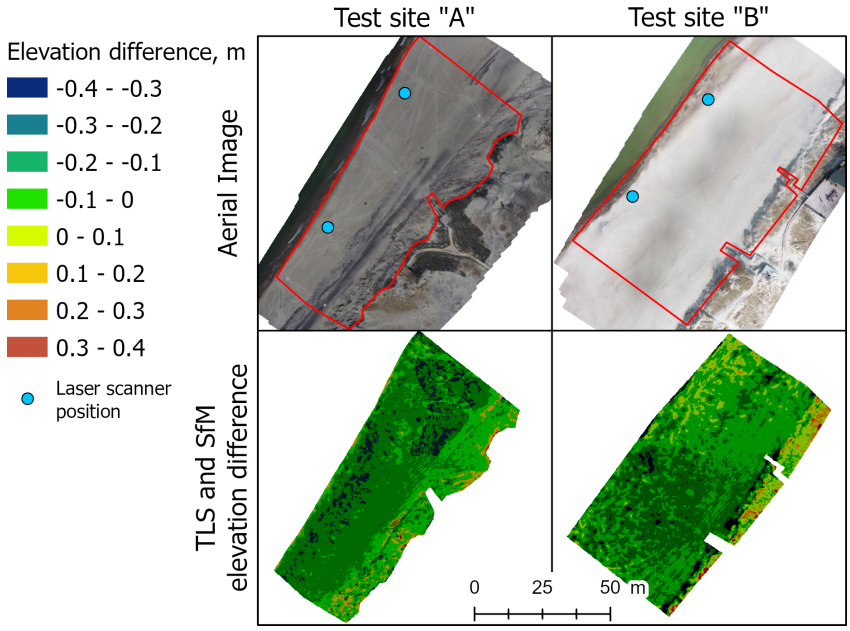

Figure 5. DEM of difference result. A – test site "A"; B – test site "B".

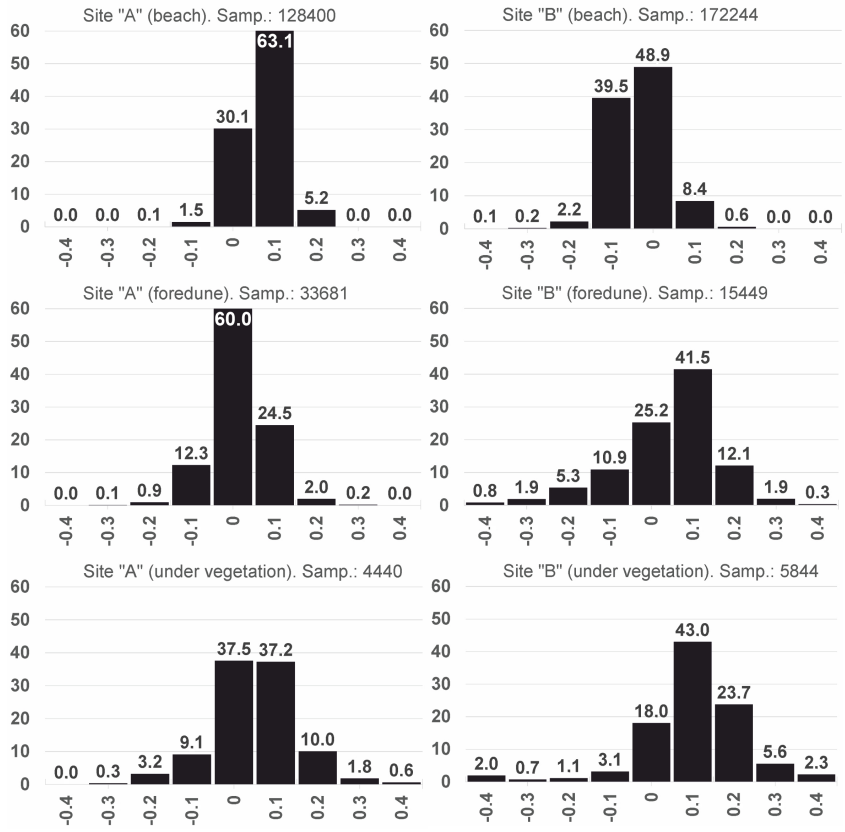

Figure 6. Histograms of elevation errors over the beach, foredune and under vegetation in the both test sites (intervals are similar to intervals in Figure 5).

error margins in height measurements, which eventually compensated for the large error margins (more than 0.2 or less than −0.2). Average negative and positive errors per area were also calculated, none of which exceeded 0.5 m even in areas with vegetation.

However, the accuracy of the digital beach models and foredune was not consistent, as seen in Figures 5 and 6 which show varying error ranges from −0.5 m to 0.5 m (Table 4).

Table 4. Statistics of the elevation errors between SfM and TLS (in meters)

Indicator	site "A"			site "B"		
	beach	foredune	under vegetation	beach	foredune	under vegetation
Count	128,400	33,681	4440	172,244	15,449	5844
Average	0.021	−0.035	−0.002	−0.035	−0.008	0.05
Std. Dev.	0.051	0.064	0.070	0.063	0.085	0.111
RMSE	0.044	0.057	0.074	0.092	0.091	0.11
Min.	−0.28	−0.31	−0.39	−0.41	−0.43	−0.49
Max.	0.25	0.34	0.41	0.21	0.40	0.47

For the beach site marked "B" in Figure 6, there was a 9% error rate of over 0.1 m, with errors more than 0.2 m occupying 268 m^2 (Figure 6). In test site "B", more than 60% of DOD cells had errors greater than 0.1 m or less than -0.1 m, appearing in mosaic patterns throughout the area (Figure 5).

There was no significant relationship between slope and height error (r^2 between 0.05 and 0.09), as previously observed in *Westoby et al.* [2012] study. It was also found that there was no significant correlation between relief curvature and elevation errors, even with the use of a sliding window size of 3×3 cells and the methods of *Zevenbergen and Thorne* [1987] in SAGA GIS 2.2.5 [*Olaya*, 2009]. All r^2 values in the calculations were less than 0.14, indicating an insignificant relationship between them.

Based on the results obtained, as well as findings from other researchers, it can be concluded that using UAVs with SfM algorithms is justifiable for shore research. The equipment is relatively easy to set up and operate, cost-effective and allows for obtaining dense point clouds for further analysis. Compared to TLS, the lightweight nature of portable UAV equipment (in our case, the field equipment set for aerial photography weighed 5 kg, versus the TLS set weighing 30 kg) is a clear advantage, facilitating manual equipment transportation to remote research sites. However, the accuracy of results is still a debated issue since statistical values such as mean error and RMSE do not provide convincing evidence against the backdrop of significant variation in height error and frequency of occurrence obtained from TLS. The spatial mosaic of height error zones also shows a clear increase in errors in the foredune ridge area.

The accuracy of obtaining and constructing DEM can be used for rapid post-storm surveys, where changes in the elevation of beaches and foredunes on shallow sandy beaches can be characterized by values up to 1.5 m [*Danchenkov and Belov*, 2019], with an error of 5–7% of the sandy material dynamics. However, for smaller mass transfer processes such as irregular aeolian movement of sandy beach material to the foredune foot, with a dry sand flow speed of $0.016–1.836 \times 10^{-2}$ kg/(m s) [*Rotnicka*, 2013], the thickness of the sand accumulation layer can only be correlated with an error extent of 50–80%, making the method not completely suitable for short-term micromorpholithodynamic studies on shallow sandy shores. It is important to study the systematic nature of errors when using UAV and SfM in the closest details, by quasi synchronous orthophotographing in natural conditions and comparing with other more precise methods of elevation measurements (total stations, TLS, level, or even by DEM control on fixed points).

Acknowledgments. The study was done with a support of the state assignment of IO RAS (Theme FMWE-2021-0012).

References

Abellán, A., J. M. Vilaplana, J. Calvet, D. García-Sellés, and E. Asensio (2011), Rockfall monitoring by Terrestrial Laser Scanning - case study of the basaltic rock face at Castellfollit de la Roca (Catalonia, Spain), *Natural Hazards and Earth System Sciences*, *11*(3), 829–841, https://doi.org/10.5194/nhess-11-829-2011.

Abellán, A., J. Vilaplana, and J. Martínez (2006), Application of a long-range Terrestrial Laser Scanner to a detailed rockfall study at Vall de Núria (Eastern Pyrenees, Spain), *Engineering Geology*, *88*(3), 136–148, https://doi.org/https://doi.org/10.1016/j.enggeo.2006.09.012.

Agisoft (2018), *Agisoft Photoscan User Manual*, *Professional Edition*, *Version 1.4*, 121 pp., Agisoft LLC.

Badyukova, E. N., L. A. Zhindarev, S. A. Lukyanova, and G. D. Solovieva (2017), Large accumulative forms of relief on the southeastern coast of the Baltic Sea, *Oceanology*, *57*(4), 580–588, https://doi.org/10.1134/s0001437017040026.

Bienert, A., S. Scheller, E. Keane, G. Mullooly, and F. Mohan (2006), Application of terrestrial laser scanners for the determination of forest inventory parameters, *International Archives of Photogrammetry, Remote Sensing and Spatial Information Sciences*, *36*(5), 1–5.

Bobykina, V. P., and Z. I. Stont (2014), Comparison of influence of strong storms of 2007 and 2012 on the coasts of the Curonian Spit, in *Problems of explore and conservation natural and cultural heritage of the national park «Curonian Spit»*, 10, pp. 173–182, IK BFU, Kaliningrad (in Russian).

Bobykina, V. P., and Z. I. Stont (2015), Winter storm activity in 2011-2012 and its consequences for the Southeastern Baltic coast, *Water Resources*, *42*(3), 371–377, https://doi.org/10.1134/s0097807815030021.

Boldyrev, V. L., V. P. Bobykina, and E. M. Burnashov (2008), State of the Curonian Spit coast after the winter storm period, in *Problems of explore and conservation natural and cultural heritage of the national park «Curonian Spit»*, 6, pp. 105–114, IK BFU, Kaliningrad (in Russian).

Brasington, J., D. Vericat, and I. Rychkov (2012), Modeling river bed morphology, roughness, and surface sedimentology using high resolution terrestrial laser scanning, *Water Resources Research*, *48*(11), https://doi.org/10.1029/2012wr012223.

Chang, K. T., H. M. Fang, S. S. Hsiao, and C. S. Li (2021), Beach Topographic Change Analysis Using Multi-temporal UAV Data, *IOP Conference Series: Earth and Environmental Science*, *799*(1), 012,022, https://doi.org/10.1088/1755-1315/799/1/012022.

Clapuyt, F., V. Vanacker, and K. V. Oost (2016), Reproducibility of UAV-based earth topography reconstructions based on Structure-from-Motion algorithms, *Geomorphology*, *260*, 4–15, https://doi.org/10.1016/j.geomorph.2015.05.011.

Collins, B. D., and N. Sitar (2005), Monitoring of Coastal Bluff Stability Using High Resolution 3 D Laser Scanning, in *Site Characterization and Modeling*, pp. 1–11, American Society of Civil Engineers, https://doi.org/10.1061/40785(164)5.

Colomina, I., and P. Molina (2014), Unmanned aerial systems for photogrammetry and remote sensing: A review, *ISPRS Journal of Photogrammetry and Remote Sensing*, *92*, 79–97, https://doi.org/10.1016/j.isprsjprs.2014.02.013.

Cook, K. L. (2017), An evaluation of the effectiveness of low-cost UAVs and structure from motion for geomorphic change detection, *Geomorphology*, *278*, 195–208, https://doi.org/10.1016/j.geomorph.2016.11.009.

Coveney, S., and A. S. Fotheringham (2011), Terrestrial laser scan error in the presence of dense ground vegetation, *The Photogrammetric Record*, *26*(135), 307–324, https://doi.org/10.1111/j.1477-9730.2011.00647.x.

Danchenkov, A. (2016), Modern technology in dune complexes monitoring on the Vistula spit, in *Proceedings of International Conference "Managinag risks to coastal regions and communities in a changinag world" (EMECS'11 - SeaCoasts XXVI)*, https://doi.org/10.31519/conferencearticle_5b1b93b8dc3ab4.15459971.

Danchenkov, A., N. Belov, and Z. Stont (2019), Using the terrestrial laser scanning technique for aeolian sediment transport assessment in the coastal zone in seasonal scale, *Estuarine, Coastal and Shelf Science*, *223*, 105–114, https://doi.org/10.1016/j.ecss.2019.04.044.

Danchenkov, A., N. Belov, E. Bubnova, and S. Myslenkov (2023), Foredune defending role: Vulnerability and potential risk through combined satellite and hydrodynamics approach, *Remote Sensing Applications: Society and Environment*, *30*, 100,934, https://doi.org/10.1016/j.rsase.2023.100934.

Danchenkov, A. R., and N. S. Belov (2019), Morphological changes in the beach-foredune system caused by a series of storms. Terrestrial laser scanning evaluation, *Russian Journal of Earth Sciences*, *19*(4), 1–14, https://doi.org/10.2205/2019ES000665.

Delacourt, C., P. Allemand, M. Jaud, P. Grandjean, A. Deschamps, J. Ammann, V. Cuq, and S. Suanez (2009), DRELIO: An Unmanned Helicopter for Imaging Coastal Areas, in *Special Issue No. 56. Proceedings of the 10th International Coastal Symposium ICS 2009*, vol. II, pp. 1489–1493.

Dudzińska-Nowak, J., and P. Wężyk (2014), Volumetric changes of a soft cliff coast 2008–2012 based on DTM from airborne laser scanning (Wolin Island, southern Baltic Sea), *Journal of Coastal Research*, *70*, 59–64, https://doi.org/10.2112/si70-011.1.

Eisenbeiss, H. (2011), The potential of unmanned aerial vehicles for mapping, in *Photogrammetric Week'11*, pp. 135–145, Wichmann-Verlag, Heidelberg.

Fabbri, S., B. M. S. Giambastiani, F. Sistilli, F. Scarelli, and G. Gabbianelli (2017), Geomorphological analysis and classification of foredune ridges based on Terrestrial Laser Scanning (TLS) technology, *Geomorphology*, *295*, 436–451, https://doi.org/10.1016/j.geomorph.2017.08.003.

Furukawa, Y., and J. Ponce (2010), Accurate, Dense, and Robust Multiview Stereopsis, *IEEE Transactions on Pattern Analysis and Machine Intelligence*, *32*(8), 1362–1376, https://doi.org/10.1109/tpami.2009.161.

Gonçalves, J. A., and R. Henriques (2015), UAV photogrammetry for topographic monitoring of coastal areas, *ISPRS Journal of Photogrammetry and Remote Sensing*, *104*, 101–111, https://doi.org/10.1016/j.isprsjprs.2015.02.009.

Haala, N. (2009), Comeback of digital image matching, in *Photogrammetric Week'09*, pp. 289–301, Wichmann-Verlag, Heidelberg.

Haala, N., M. Cramer, and M. Rothermel (2013), Quality of 3D point clouds from highly overlapping UAV Imagery, *The International Archives of the Photogrammetry, Remote Sensing and Spatial Information Sciences*, *XL-1/W2*, 183–188, https://doi.org/10.5194/isprsarchives-xl-1-w2-183-2013.

Hengl, T. (2006), Finding the right pixel size, *Computers & Geosciences*, *32*(9), 1283–1298, https://doi.org/10.1016/j.cageo.2005.11.008.

Hodge, R., J. Brasington, and K. Richards (2009), In situ characterization of grain-scale fluvial morphology using Terrestrial Laser Scanning, *Earth Surface Processes and Landforms*, pp. 954–968, https://doi.org/10.1002/esp.1780.

James, L. A., M. E. Hodgson, S. Ghoshal, and M. M. Latiolais (2012), Geomorphic change detection using historic maps and DEM differencing: The temporal dimension of geospatial analysis, *Geomorphology*, *137*(1), 181–198, https://doi.org/10.1016/j.geomorph.2010.10.039.

James, M. R., and S. Robson (2012), Straightforward reconstruction of 3D surfaces and topography with a camera: Accuracy and geoscience application, *Journal of Geophysical Research: Earth Surface*, *117*(F3), https://doi.org/10.1029/2011jf002289.

Jeyaraj, S., B. Ramakrishnan, and R. Ramsankaran (2022), Application of Unmanned Aerial Vehicle (UAV) in the assessment of beach volume change-A case study of Malgund beach, in *OCEANS 2022 - Chennai*, pp. 1–14, IEEE, https://doi.org/10.1109/oceanschennai45887.2022.9775290.

Johnson, K., E. Nissen, S. Saripalli, J. R. Arrowsmith, P. McGarey, K. Scharer, P. Williams, and K. Blisniuk (2014), Rapid mapping of ultrafine fault zone topography with structure from motion, *Geosphere*, *10*(5), 969–986, https://doi.org/10.1130/ges01017.1.

Kempeneers, P., B. Deronde, S. Provoost, and R. Houthuys (2009), Synergy of Airborne Digital Camera and Lidar Data to Map Coastal Dune Vegetation, *Journal of Coastal Research*, *25*(6), 73–82.

Kirlis, V. I. (1971), Some peculiarities of seashore dynamics of the Kursiu-Nerija barrier, *4*(67), 211–224.

Lane, S. N., T. D. James, and M. D. Crowell (2000), Application of Digital Photogrammetry to Complex Topography for Geomorphological Research, *The Photogrammetric Record*, *16*(95), 793–821, https://doi.org/10.1111/0031-868x.00152.

Lee, H., S. Lim, and D. Park (2011), Application of terrestrial laser scanner and raster operations to change detection of beach, *Journal of Coastal Research*, pp. 1692–1696.

Lee, H.-S., I.-H. Kim, and H.-G. Kim (2016), Application of Terrestrial 3D Laser Scanning to Monitor Changes of Beach Landforms, *Journal of Coastal Research*, *75*(sp1), 173–177, https://doi.org/10.2112/si75-035.1.

Milan, D. J., G. L. Heritage, and D. Hetherington (2007), Application of a 3D laser scanner in the assessment of erosion and deposition volumes and channel change in a proglacial river, *Earth Surface Processes and Landforms*, *32*(11), 1657–1674, https://doi.org/10.1002/esp.1592.

Milan, D. J., G. L. Heritage, A. R. G. Large, and I. C. Fuller (2011), Filtering spatial error from DEMs: Implications for morphological change estimation, *Geomorphology*, *125*(1), 160–171, https://doi.org/10.1016/j.geomorph.2010.09.012.

Mitasova, H., M. Overton, and R. S. Harmon (2005), Geospatial analysis of a coastal sand dune field evolution: Jockey's ridge, north carolina, *Geomorphology*, *72*(1), 204–221, https://doi.org/https://doi.org/10.1016/j.geomorph.2005.06.001.

Mitasova, H., M. F. Overton, J. J. Recalde, D. J. Bernstein, and C. W. Freeman (2009), Raster-Based Analysis of Coastal Terrain Dynamics from Multitemporal Lidar Data, *Journal of Coastal Research*, *25*(2), 507–514.

Morozov, A. F., and O. V. Petrov (2010), *Atlas of Geological and Environmental Geological Maps of the Russian Area of the Baltic Sea*, 78 pp., VSEGEI (in Russian).

Neitzel, F., and J. Klonowski (2011), Mobile 3D mapping with a low-cost UAV system, *The International Archives of the Photogrammetry, Remote Sensing and Spatial Information Sciences*, *XXXVIII-1/C22*, 39–44, https://doi.org/10.5194/isprsarchives-xxxviii-1-c22-39-2011.

Nex, F., and F. Remondino (2013), UAV for 3D mapping applications: a review, *Applied Geomatics*, *6*(1), 1–15, https://doi.org/10.1007/s12518-013-0120-x.

Nocerino, E., F. Menna, F. Remondino, and R. S. Lunazzi (2013), Accuracy and Block Deformation Analysis in Automatic UAV and Terrestrial Photogrammetry - Lesson Learnt, *ISPRS Annals of the Photogrammetry, Remote Sensing and Spatial Information Sciences*, *II-5/W1*, 203–208, https://doi.org/10.5194/isprsannals-ii-5-w1-203-2013.

Obanawa, H., Y. S. Hayakawa, H. Satio, and C. Gomez (2014), Comparison of DSMs derived from UAV-SfM method and terrestrial laser scanning, *Journal of the Japan society of photogrammetry and remote sensing*, *53*(2), 67–74, https://doi.org/10.4287/jsprs.53.67.

Olaya, V. (2009), Chapter 6 Basic Land-Surface Parameters, in *Developments in Soil Science*, vol. 33, pp. 141–169, Elsevier, https://doi.org/10.1016/s0166-2481(08)00006-8.

Pe'eri, S., and B. Long (2011), LIDAR technology applied in coastal studies and management, *Journal of Coastal Research*, *62*, 1–5, https://doi.org/10.2112/si_62_1.

Pierrot Deseilligny, M., and I. Clery (2011), APERO, an Open Source Bundle Adjusment Software for Automatic Calibration and Orientation of Set of Images, *The International Archives of the Photogrammetry, Remote Sensing and Spatial Information Sciences*, *XXXVIII-5/W16*, 269–276, https://doi.org/10.5194/isprsarchives-XXXVIII-5-W16-269-2011.

Poulton, C. V. L., J. Lee, P. Hobbs, L. Jones, and M. Hall (2006), Preliminary investigation into monitoring coastal erosion using terrestrial laser scanning: case study at Happisburgh, Norfolk, *Bulletin of the Geological Society of Norfolk*, *56*, 45–64.

Puliti, S., H. Ørka, T. Gobakken, and E. Næsset (2015), Inventory of Small Forest Areas Using an Unmanned Aerial System, *Remote Sensing*, *7*(8), 9632–9654, https://doi.org/10.3390/rs70809632.

Remondino, F., L. Barazzetti, F. Nex, M. Scaioni, and D. Sarazzi (2011), UAV photogrammetry for mapping and 3D modeling – current status and future perspectives, *The International Archives of the Photogrammetry, Remote Sensing and Spatial Information Sciences*, *XXXVIII-1/C22*, 25–31, https://doi.org/10.5194/isprsarchives-xxxviii-1-c22-25-2011.

Rinaudo, F., F. Chiabrando, A. Lingua, and A. Spanò (2012), Archaeological site monitoring: UAV photogrammetry can be an answer, *The International Archives of the Photogrammetry, Remote Sensing and Spatial Information Sciences*, *XXXIX-B5*, 583–588, https://doi.org/10.5194/isprsarchives-xxxix-b5-583-2012.

Rotnicka, J. (2013), Aeolian vertical mass flux profiles above dry and moist sandy beach surfaces, *Geomorphology*, *187*, 27–37, https://doi.org/10.1016/j.geomorph.2012.12.032.

Rowlands, K. A., L. D. Jones, and M. Whitworth (2003), Landslide Laser Scanning: a new look at an old problem, *Quarterly Journal of Engineering Geology and Hydrogeology*, *36*(2), 155–157, https://doi.org/10.1144/1470-9236/2003-08.

Sallenger Jr., A. H., W. B. Krabill, R. N. Swift, J. Brock, J. List, M. Hansen, R. A. Holman, S. Manizade, J. Sontag, A. Meredith, K. Morgan, J. K. Yunkel, E. B. Frederick, and H. Stockdon (2003), Evaluation of Airborne Topographic Lidar for Quantifying Beach Changes, *Journal of Coastal Research*, *19*(1), 125–133.

Sergeev, A., D. Ryabchuk, V. Zhamoida, and I. Leont'ev (2016), Application of onshore laser scanning data for mathematic modeling of coastal profile changes, in *Proceedings of International Conference "Managinag risks to coastal regions and communities in a changinag world" (EMECS'11 - SeaCoasts XXVI)*, Academus Publishing, https://doi.org/10.31519/conferencearticle_5b1b943d5666e6.34864386.

Sibson, R. (1981), A Brief Description of Natural Neighbor Interpolation, in *Interpreting Multivariate Data*, pp. 21–36, John Wiley & Sons, New York.

Snavely, N., S. M. Seitz, and R. Szeliski (2007), Modeling the World from Internet Photo Collections, *International Journal of Computer Vision*, *80*(2), 189–210, https://doi.org/10.1007/s11263-007-0107-3.

Stont, Z. I. (2014), *Current trends in the hydro-meteorological parameters of the South-East Baltic and their effect on coastal processes. An abstract of a PhD thesis*, 22 pp., IK BFU, Kaliningrad (in Russian).

Stont, Z. I., A. Y. Sergeev, and M. O. Ulyanova (2020), Dynamics Of Dune Massifs In Various Meteorological Conditions On The Example Of The Curonian Spit (South-Eastern Baltic Sea Coast), *Geography, Environment, Sustainability*, *13*(3), 57–67 (in Russian).

Topcon (2010), *Instruction manual, laser scanner GLS-1500 series*, 88 pp., Topcon corporation.

Travelletti, J., T. Oppikofer, C. Delacourt, J.-P. Malet, and M. Jaboyedoff (2008), Monitoring landslide displacements during a controlled rain experiment using a long-range terrestrial laser scanning (TLS), in *The International Archives of the Photogrammetry, Remote Sensing and Spatial Information Sciences*, vol. 37, pp. 485–490.

Turner, D., A. Lucieer, and C. Watson (2012), An Automated Technique for Generating Georectified Mosaics from Ultra-High Resolution Unmanned Aerial Vehicle (UAV) Imagery, Based on Structure from Motion (SfM) Point Clouds, *Remote Sensing*, *4*(5), 1392–1410, https://doi.org/10.3390/rs4051392.

Turner, I. L., M. D. Harley, and C. D. Drummond (2016), UAVs for coastal surveying, *Coastal Engineering*, *114*, 19–24, https://doi.org/10.1016/j.coastaleng.2016.03.011.

Westaway, R. M., S. N. Lane, and D. M. Hicks (2000), The development of an automated correction procedure for digital photogrammetry for the study of wide, shallow, gravel-bed rivers, *Earth Surface Processes and Landforms*, *25*(2), 209–226, https://doi.org/10.1002/(sici)1096-9837(200002)25:2<209::aid-esp84>3.0.co;2-z.

Westoby, M. J., J. Brasington, N. F. Glasser, M. J. Hambrey, and J. M. Reynolds (2012), 'Structure-from-Motion' photogrammetry: A low-cost, effective tool for geoscience applications, *Geomorphology*, *179*, 300–314, https://doi.org/10.1016/j.geomorph.2012.08.021.

White, S. A., and Y. Wang (2003), Utilizing DEMs derived from LIDAR data to analyze morphologic change in the North Carolina coastline, *Remote Sensing of Environment*, *85*(1), 39–47, https://doi.org/https://doi.org/10.1016/S0034-4257(02)00185-2.

Xhardé, R., B. F. Long, and D. L. Forbes (2011), Short-Term Beach and Shoreface Evolution on a Cuspate Foreland Observed with Airborne Topographic and Bathymetric LIDAR, *Journal of Coastal Research*, *62*, 50–61, https://doi.org/10.2112/si_62_6.

Zanutta, A., A. Lambertini, and L. Vittuari (2020), UAV Photogrammetry and Ground Surveys as a Mapping Tool for Quickly Monitoring Shoreline and Beach Changes, *Journal of Marine Science and Engineering*, *8*(1), 52, https://doi.org/10.3390/jmse8010052.

Zevenbergen, L. W., and C. R. Thorne (1987), Quantitative analysis of land surface topography, *Earth Surface Processes and Landforms*, *12*(1), 47–56, https://doi.org/10.1002/esp.3290120107.